



HAL
open science

Symmetry-broken perturbation theory to large orders in antiferromagnetic phases

Renaud Garioud, Fedor Šimkovic, Riccardo Rossi, Gabriele Spada, Thomas Schäfer, Félix Werner, Michel Ferrero

► **To cite this version:**

Renaud Garioud, Fedor Šimkovic, Riccardo Rossi, Gabriele Spada, Thomas Schäfer, et al.. Symmetry-broken perturbation theory to large orders in antiferromagnetic phases. 2023. hal-04309847

HAL Id: hal-04309847

<https://hal.science/hal-04309847>

Preprint submitted on 27 Nov 2023

HAL is a multi-disciplinary open access archive for the deposit and dissemination of scientific research documents, whether they are published or not. The documents may come from teaching and research institutions in France or abroad, or from public or private research centers.

L'archive ouverte pluridisciplinaire **HAL**, est destinée au dépôt et à la diffusion de documents scientifiques de niveau recherche, publiés ou non, émanant des établissements d'enseignement et de recherche français ou étrangers, des laboratoires publics ou privés.

Symmetry-broken perturbation theory to large orders in antiferromagnetic phases

Renaud Garioud^{1,2,*}, Fedor Šimkovic IV^{1,2}, Riccardo Rossi^{3,4},

Gabriele Spada^{5,6}, Thomas Schäfer⁷, Félix Werner⁵, and Michel Ferrero^{1,2}

¹CPHT, CNRS, Ecole Polytechnique, Institut Polytechnique de Paris, Route de Saclay, 91128 Palaiseau, France

²Collège de France, 11 place Marcelin Berthelot, 75005 Paris, France

³Institute of Physics, École Polytechnique Fédérale de Lausanne (EPFL), CH-1015 Lausanne, Switzerland

⁴Sorbonne Université, CNRS, Laboratoire de Physique Théorique de la Matière Condensée, LPTMC, F-75005 Paris, France

⁵Laboratoire Kastler Brossel, École Normale Supérieure - Université PSL,

CNRS, Sorbonne Université, Collège de France, 75005 Paris, France

⁶INO-CNR BEC Center and Dipartimento di Fisica, Università di Trento, 38123 Trento, Italy

⁷Max-Planck-Institut für Festkörperforschung, Heisenbergstraße 1, 70569 Stuttgart, Germany

(Dated: June 28, 2023)

We introduce a spin-symmetry-broken extension of the connected determinant algorithm [Phys. Rev. Lett. 119, 045701 (2017)]. The resulting systematic perturbative expansions around an antiferromagnetic state allow for numerically exact calculations directly inside a magnetically ordered phase. We show new precise results for the magnetic phase diagram and thermodynamics of the three-dimensional cubic Hubbard model at half-filling. With detailed computations of the order parameter in the low to intermediate-coupling regime, we establish the Néel phase boundary. The critical behavior in its vicinity is shown to be compatible with the $O(3)$ Heisenberg universality class. By determining the evolution of the entropy with decreasing temperature through the phase transition we identify the different physical regimes at $U/t=4$. We provide quantitative results for several thermodynamic quantities deep inside the antiferromagnetic dome up to large interaction strengths and investigate the crossover between the Slater and Heisenberg regimes.

In strongly correlated materials, such as high temperature superconducting copper oxides or iron-based pnictides, the interactions between electrons yield intricate phase diagrams, exhibiting, e.g., magnetically or charge-ordered phases, superconductivity or Mott insulating behaviors. Understanding the properties of these different phases, their interplay and driving mechanisms is one of the outstanding challenges of modern condensed matter theory.

From the theoretical point of view, one of the simplest models to investigate phase transitions is the three-dimensional cubic Hubbard model [1–6] given by the Hamiltonian

$$\hat{\mathcal{H}} = -t \sum_{\langle i,j \rangle} \sum_{\sigma} \hat{c}_{i\sigma}^{\dagger} \hat{c}_{j\sigma} + U \sum_i \hat{n}_{i\uparrow} \hat{n}_{i\downarrow} - \mu \sum_{i\sigma} \hat{n}_{i\sigma}, \quad (1)$$

where t is the hopping amplitude between nearest-neighbor sites $\langle i, j \rangle$ on a cubic lattice, $U \geq 0$ the on-site Coulomb interaction, μ the chemical potential, $\hat{n}_{i\sigma} = \hat{c}_{i\sigma}^{\dagger} \hat{c}_{i\sigma}$ and $\hat{c}_{i\sigma}^{\dagger}$ creates an electron on site i with spin σ . At half-filling ($\mu = U/2$), the ground state has antiferromagnetic long-range spin order. In three dimensions this $SU(2)$ symmetry-broken phase survives up to the Néel temperature $T_N(U)$ above which the system becomes paramagnetic. While there is qualitative understanding of the mechanisms that produce the antiferromagnetic order both at weak and strong coupling, obtaining unbiased quantitative results, especially close to the phase transition and inside the ordered phase, is still very challenging [7–17]. Therefore, despite its apparent simplicity, the Hubbard model on the cubic lattice is an ideal platform to explore the potential of new algorithms

before engaging in the study of more realistic systems. The model was realized in cold-atomic experiments on optical lattices where antiferromagnetism is under active investigation [18–26].

The main challenge for theoretical approaches based on finite size lattices is to properly account for the increasing correlation length in the vicinity of a second order phase transition, and, as such, to extrapolate to the thermodynamic limit. In that respect, the diagrammatic Monte Carlo approach [27–29] is very promising as it offers the possibility to investigate a system directly in the thermodynamic limit. The method stochastically computes the coefficients a_k appearing in the perturbative expansion in U of a physical observable, $\mathcal{A}(U) = \sum_k a_k U^k$ in the simplest formulation. The computational cost rapidly increases with increasing perturbation orders and only so many coefficients can be computed before the statistical variance becomes overwhelming. Nevertheless, important improvements [30, 31] make it now possible to reach perturbation orders as large as 10–12. In the context of the repulsive Hubbard model, diagrammatic Monte Carlo has already been successfully applied to non-perturbative regimes in the two-dimensional square lattice [29, 32–41].

In the usual formulation, the perturbation series is constructed starting from the non-interacting ($U = 0$) $SU(2)$ -symmetric solution of Eq. (1). This allows to obtain results for the interacting system in its paramagnetic regime. As the phase transition to the antiferromagnetic state is approached, however, the resummation of the series becomes increasingly difficult. The reason is that a second-order phase transition happening at $U = U_c$ is accompanied by a singularity in the complex- U plane

for observables $\mathcal{A}(U)$ that show a non-analyticity at U_c . Consequently, investigating the antiferromagnetic transition in the cubic Hubbard model can only be done from temperatures above and not too close to the Néel temperature T_N . Very recently, the spin structure factor perturbation series has been computed this way in the paramagnetic phase of the cubic Hubbard model [40]. Assuming the critical behavior in the vicinity of the phase transition, the authors were able to accurately compute T_N in the weak-to-intermediate coupling regime both at half-filling and at finite doping. This approach is however not able to address the properties of the model inside the ordered phase.

In this Letter, we take a complementary approach and compute the perturbation series for physical observables within the antiferromagnetic phase of the cubic half-filled Hubbard model. We show that our broken-symmetry approach to perturbative expansions is a powerful tool for studying magnetically ordered phases and phase transitions. Our results are obtained directly in the thermodynamic limit and, thus, do not involve any finite size scaling. We document the vanishing of the magnetic order parameter at T_N and the corresponding critical exponent β and report and discuss the behavior of the double occupancy, grand potential and entropy across the phase transition and inside the ordered phase.

Method. The possibility to construct symmetry-broken perturbation series comes from a flexibility in the choice of the starting point around which the perturbation is expanded. This freedom has been extensively applied to diagrammatic Monte Carlo computations in the non-magnetic phase to improve the convergence properties of the series [37–39, 42–50]. Very recently, it has been used to construct a perturbation theory around a BCS state and inside the superconducting phase of the attractive Hubbard model [51]. Here, we follow similar steps and introduce the modified Hamiltonian

$$\hat{\mathcal{H}}_\xi = -t \sum_{\langle i,j \rangle} \sum_{\sigma} \hat{c}_{i\sigma}^\dagger \hat{c}_{j\sigma} - \xi \frac{U}{2} \sum_{i\sigma} \hat{n}_{i\sigma} + (1-\xi)h \sum_i p_i \hat{S}_i^z + \xi U \sum_i \hat{n}_{i\uparrow} \hat{n}_{i\downarrow}, \quad (2)$$

where $\hat{S}_i^z = (\hat{n}_{i\uparrow} - \hat{n}_{i\downarrow})/2$ and $p_i = \pm 1$ depending on whether i belongs to one or the other sub-lattice of the bipartite cubic lattice. Observables are expressed as perturbation series in ξ and physical results are recovered for $\xi = 1$ where both Hamiltonians become equivalent, $\hat{\mathcal{H}}_{\xi=1} = \hat{\mathcal{H}}$. The perturbation series in ξ is built around a state that breaks the $SU(2)$ spin rotation symmetry of the original Hamiltonian. Indeed, $\hat{\mathcal{H}}_{\xi=0}$ describes free electrons in a staggered external magnetic field h . Because this state breaks the symmetry from the start, the perturbation series can describe a magnetically ordered phase without the need of undergoing a phase transition. Accordingly, singularities in the complex- ξ plane associ-

ated to the phase transition are avoided.

We compute the coefficients of the perturbation series with the CDet [30] algorithm using a rejection-free many-configuration Monte Carlo [52] as well as a fast principal minor algorithm [53, 54] to improve the speed of the determinant calculations. The series are evaluated with different resummation techniques [55, 56] that serve as a basis to determine the error bars of our results, see Supplementary Material [57]. While the diagrammatic expansion can be formulated directly in the thermodynamic limit, in practice, we use a system with $L^3 = 20^3$ sites for our computations. We have carefully checked that this is large enough to avoid finite-size effects, even in the vicinity of the phase transition, as discussed in the Supplementary Material [57]. In the following, we will denote this spin symmetry-broken algorithm by CDet(AF).

In the Hamiltonian of Eq. (2), the field h can be chosen arbitrarily and different choices for h define different series. In order to obtain the best convergence and to cross-check different results, we have computed several values in the range $0 \leq h \leq h_{\text{MF}}$, where h_{MF} is the effective field found in the mean-field solution of Eq. (1). In the following, we will parameterize $h = \alpha h_{\text{MF}}$ with $0 \leq \alpha \leq 1$. Note that when $\alpha = 0$, the perturbation series is the usual expansion limited to the paramagnetic regime.

For our analysis we compute the double occupancy $D = \langle \hat{n}_{i\uparrow} \hat{n}_{i\downarrow} \rangle = E_{\text{pot}}/U$, the staggered magnetization $m = \langle \hat{n}_{i\uparrow} - \hat{n}_{i\downarrow} \rangle$ (which is the order parameter for the Néel phase transition) and the grand potential per lattice site $-\Omega/L^3 = P$ where L is the linear system size

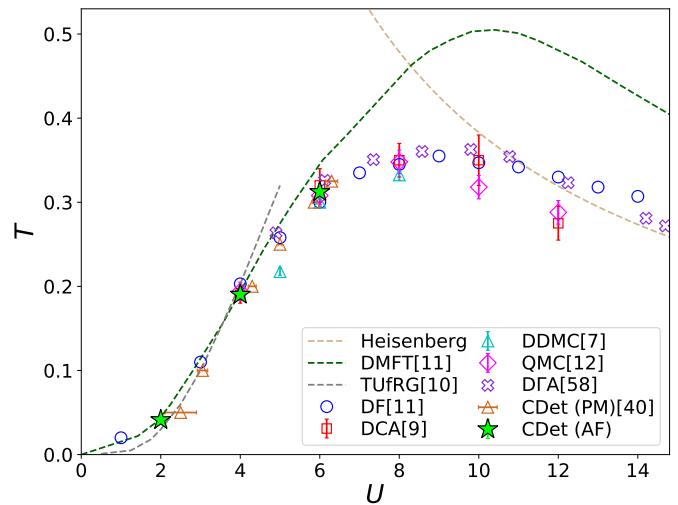


FIG. 1. Comparison of the Néel temperature $T_N(U)$ (lime stars), obtained with the symmetry broken CDet(AF), with other numerical methods. References for the numerical methods data are indicated in the legend.

of the cubic lattice, and P the thermodynamic pressure. The grand potential computations enable us to determine the entropy density and magnetization through

$$s = -\frac{\partial\Omega}{L^3\partial T} \quad m = -\left.\frac{\partial\Omega}{L^3\partial H_{\text{ext}}}\right|_{H_{\text{ext}}=0}, \quad (3)$$

where H_{ext} is an external Zeeman staggered field whose sign alternates on neighboring sites in the form of an additional term to the Hubbard Hamiltonian Eq. (1): $H_{\text{ext}} \sum_i p_i \hat{S}_i^z$. All energies are expressed in units of the hopping amplitude $t=1$.

Phase diagram and universality class. We start our study by determining the Néel temperature for different values of the interaction in order to establish the magnetic phase diagram of the system.

In Fig. 1 we compare our values for the critical temperature $T_N(U)$ from CDet(AF) against numerous other numerical methods [7, 9–12, 40, 58]. The Néel temperature is expected to increase with increasing interaction at small U since the transition is driven by the Slater mechanism [59] and reaches a maximum in the intermediate coupling around $U \simeq 6-10$, before decreasing like $T_N \simeq 0.946J$ [60] in the high- U Heisenberg limit, where $J = 4t^2/U$ is the super-exchange coupling. We have been able to determine the critical temperature up to an intermediate coupling strength of $U = 6$. For $U > 6$, regarding the magnetization, we experience increased difficulty in resumming our perturbation series and loss of Monte Carlo accuracy in the critical region close to the phase transition.

The values of the Néel temperature displayed in Fig. 1 are obtained from the computation of the magnetization as a function of temperature $m(T)$, which we show in Fig. 2. The order parameter m indicates the phase transition by assuming a non-zero value when decreasing the temperature: $T_N(U=2) = 0.0425(25)$, $T_N(U=4) = 0.1925(25)$ and $T_N(U=6) = 0.3125(25)$. Thanks to our high precision data, we manage to compute directly the β critical exponent from the critical behaviour $m(T) \simeq a(T_N - T)^\beta$. The obtained values for the critical exponent Fig. 2 (top right) compare remarkably well to the literature values for the $O(3)$ Heisenberg universality class [8, 11, 61, 62]. They establish the first direct computations of the β critical exponent on a fermionic lattice and in the thermodynamic limit. As shown in Fig. 1, the values that we obtain for the Néel temperature compare well with paramagnetic DiagMC [40] and DCA extrapolated to infinite cluster size [9], as well as to the recently improved dynamical vertex approximation DGA [58], but are out of the error bounds obtained by finite-size scaling of $L \leq 10$ DDMC data [7]. The critical region, defined as the temperature range $T \in [T_N - \delta T, T_N]$ where $m(T) = a(T_N - T)^\beta$ is a good fit to our data, is of the order of $\delta T \simeq 0.025$ for $U \geq 4$. The magnetization and the other thermodynamic quantities (see Figs 3 and 4) only have a variation in a temperature interval $\delta T \simeq 0.1$

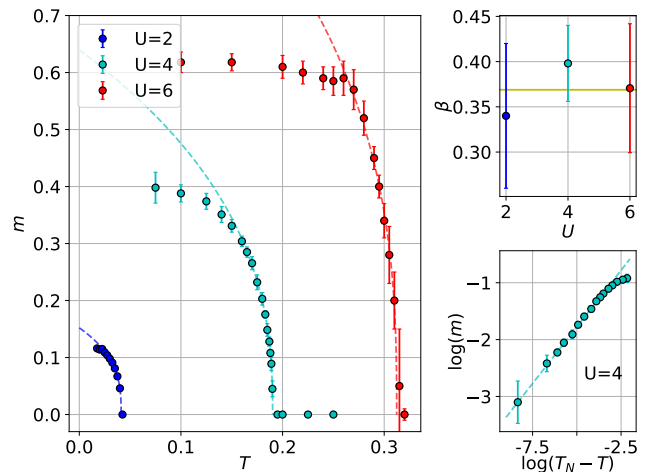


FIG. 2. Magnetization and critical behavior - Left panel: Magnetization m as a function of temperature T for three different values of the interaction U . The dashed curves represent the critical behavior as determined from our data close to the critical temperature fitted with the formula: $m(T) \simeq a(T_N - T)^\beta$. Top right panel: Critical exponent obtained from the three magnetization curves. The gold horizontal band corresponds to the theoretically predicted value of β for the $O(3)$ Heisenberg universality class in [61]. Lower right panel: magnetization as a function of $T_N - T$ at $U = 4$ on a log-log scale. T_N is determined with the critical behavior fit from the left panel. The dashed line corresponds to the fitting curve on the left panel.

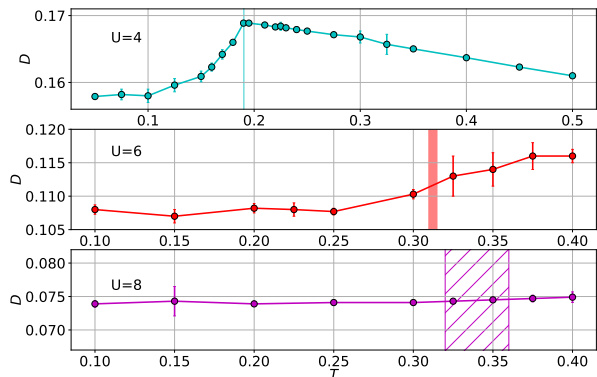


FIG. 3. Double occupancy D as a function of temperature for three different values of the interaction U . The vertical bands at $U = 4$ and $U = 6$ correspond to the estimate of the Néel temperature from our study, while the hashed area at $U = 8$ is an estimate of the Néel transition from other numerical methods displayed in Fig. 1.

below T_N before they essentially saturate to their low temperature value. This interval does not seem to expand when increasing the interaction and hence the Néel temperature for $U \geq 4$.

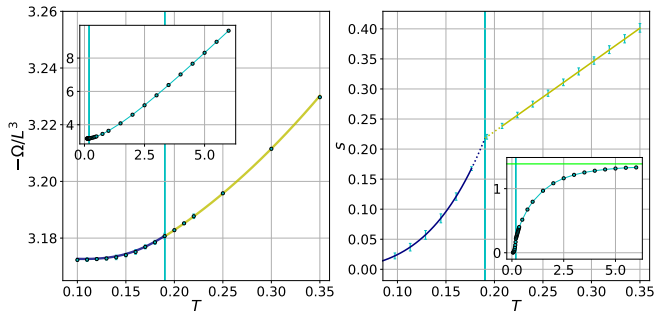


FIG. 4. Left panel: Grand potential density $-\Omega/L^3$ as a function of temperature T at interaction $U = 4$. When not visible the error bar is smaller than the markers. Right panel: Entropy density s as a function of temperature T obtained as derivative of the grand potential fitting curves (see text). The cyan error bars give the error on the entropy curve. We do not have enough data close to the Néel temperature to resolve the critical behaviour of the entropy, and the entropy curve is dashed in this region. The insets are the same plots on a larger temperature range. The lime horizontal line indicates the high temperature limit $s = \log(4)$. On both panels the vertical lines correspond to the value of the Néel temperature obtained in Fig. 2.

Double occupancy. The signatures of the phase transition can also be read from the double occupancy, shown in Fig. 3. At $U = 4$, we observe a singularity in the double occupancy at a temperature in good agreement with the value of the Néel temperature determined in Fig. 2. At this value of the interaction, the double occupancy increases with decreasing temperature in the normal phase because of the Pomeranchuk effect [63–67]. It decreases in the antiferromagnetic phase which is consistent with the Slater mechanism expected at small interaction: The ordered phase is stabilized because of a gain in potential energy $E_{pot} = UD$ and, hence, a lowering of double occupancy at fixed interaction. At higher values of U the double occupancy curve flattens, and within our accuracy, we are not able to document the non-analyticity of the double occupancy at the Néel temperature. We do not observe significant changes of the double occupancy around the Néel temperature at $U = 8$ within the 10^{-2} relative accuracy of our computation. Further work with better sensitivity or studying the kinetic energy would be needed to clearly document the change from a Slater to a Heisenberg regime with a kinetic-energy driven phase transition, as was done in DMFT and extensions thereof in [68–70].

Grand potential. The grand potential at $U = 4$ is displayed in Fig. 4. In order to evaluate the entropy density from Eq. (3) we suppose a polynomial behavior of the grand potential with temperature. Since $\Omega(T) - \Omega(T = 0) \propto T^4$ for $T \rightarrow 0$, we fit the $T < T_N$ data with the expression $-\Omega(T) = -\Omega(T=0) + aT^4 + bT^5 + cT^6$ (cyan curve). At $T > T_N$ we expect a quadratic behavior in the

degenerate Fermi liquid regime. The data is well fitted by the expression $-\Omega/L^3(T) = d + eT^2$ (yellow curve). We impose continuity up to first order derivative at $T = T_N$. At higher temperatures $T \geq 0.4$ the grand potential becomes almost linear in temperature $-\Omega(T) \simeq \log(4)T$. The entropy density is then extracted with a finite difference scheme. These different behaviors of the grand potential lead to different physical regimes for the evolution of the entropy density with temperature. In the AF phase the entropy density varies as $s \propto T^3$ at small temperatures. For temperatures just above the transition $T \in [T_N, 0.35]$ the entropy density increases linearly with the temperature which is a signature of a metallic behaviour of the system in this part of the phase diagram. At higher temperatures of the order of the interaction $T \sim U = 4$ the entropy density saturates to $s(T \rightarrow +\infty) = \log(4)$.

Magnetically saturated regime at low T . We are now interested in the low temperature properties of the system where the magnetization has reached saturation. We have observed earlier that the magnetization only changes significantly in a shell of size $\delta T \sim 0.1$ below the Néel temperature, so that the region with saturated magnetization represents an important part of the antiferromagnetic dome.

Direct computations of the magnetization become problematic for $U > 6$ because the associated series are difficult to resum. At small temperature it turns out to be more practical to compute the grand potential density and extract the magnetization as its variation with the external field as stated in Eq. (3). More details, and the associated computations are shown in [57].

The directly computed magnetization compares well with differentiating the grand potential as shown in Fig. 5. For $U \geq 6$ we observe no difference between the $T = 0.1$ and $T = 0.2$ curves which shows that the magnetization is already saturated at its zero temperature value. The magnetization will eventually have a maximum with respect to U , but this must happen for values of $U > 18$.

The variations of the double occupancy with the interaction at low temperatures are shown in Fig. 5. In the normal phase the double occupancy is decreasing quasilinearly with the interaction. In the vicinity of the phase transition we observe good agreement between results for the paramagnetic and symmetry-broken computations. As expected, at the transition U_c we observe a singularity in the double occupancy, and these results can be used to estimate the value of the critical interaction at fixed temperature. The double occupancy decreases faster with increasing interaction when entering the AF phase which is consistent with the Slater mechanism at the transition for values of the critical interaction $U_c < 6$. In the antiferromagnetic phase the double occupancy is a convex function of the interaction which decays slowly to zero at infinite interaction. At $U > 7$ we cannot distinguish

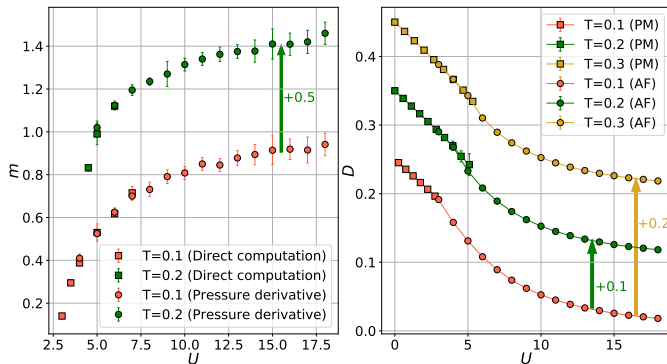


FIG. 5. Left panel: Magnetization as a function of the interaction U for two different values of the temperature. For better visibility the magnetization at $T = 0.2$ is shifted by $+0.5$. The square markers are obtained through direct computation of the order parameter like in Fig. 2. The round markers are obtained by numerically differentiating the grand potential density at an external field $H_{\text{ext}} \rightarrow 0$, see Eq. (3). Right panel: Double occupancy D as a function of the interaction U for three different values of the temperature. For better visibility the data at $T = 0.2$ ($T = 0.3$) is shifted by $+0.1$ ($+0.2$). The square markers are in the normal phase and are obtained with the paramagnetic (PM) CDet algorithm (no symmetry-breaking at $\alpha = 0$). The round markers are obtained with the antiferromagnetic symmetry-broken CDet with $\alpha \neq 0$ (AF).

between the different temperatures within our accuracy as expected from Fig. 3.

Conclusions. To conclude, we have applied the new algorithmic developments of the symmetry-broken CDet approach to produce the first high order diagrammatic computations inside an antiferromagnetic phase and directly in the thermodynamic limit. We have provided a quantitative description of the antiferromagnetic phase of the cubic half-filled Hubbard model. After determining the critical behavior of the system and its phase diagram we have reported resummed results at small temperatures deep inside the antiferromagnetic dome up to high interactions $U = 18$. We have shown that diagrammatic Monte Carlo is a powerful tool to study the physics of ordered systems with no need for an embedding scheme or system size extrapolation. A more advanced, non-linear chemical-potential shift combined with other CDet extensions [39] may lead to further improvements for describing the critical behaviour in the strong-coupling Heisenberg part of the antiferromagnetic dome. This symmetry-broken expansion could be applied to incommensurate orders in the doped regime, similarly to what was done in the normal phase [40] or with embedding methods [62]. Another interesting possibility would be to extend our study by including an anisotropic hopping term $t_{\text{perp}} < t$ in the z -direction (similarly to what was done in [71]) in order to investigate how the magnetic properties are modified as the two-dimensional limit is

approached. This application would be especially relevant for the physics of cuprate superconductors.

The authors are grateful to A. Georges, A.J. Kim, E. Kozik, C. Lenihan, G. Rohringer, and J. Stobbe for valuable discussions. This work was granted access to the HPC resources of TGCC and IDRIS under the allocations A0110510609 attributed by GENCI (Grand Equipement National de Calcul Intensif). This work has been supported by the Simons Foundation within the Many Electron Collaboration framework. High Performance Computing resources were provided by the IT support team of CPHT laboratory.

* garioudrenaud@gmail.com

- [1] J. Hubbard and Brian Hilton Flowers. Electron correlations in narrow energy bands. *Proc. R. Soc. London, Sect. A*, 276(1365):238–257, 1963. URL: <https://royalsocietypublishing.org/doi/abs/10.1098/rspa.1963.0204>, doi:10.1098/rspa.1963.0204.
- [2] J. Hubbard and Brian Hilton Flowers. Electron correlations in narrow energy bands III. An improved solution. *Proc. R. Soc. London, Sect. A*, 281(1386):401–419, 1964. URL: <https://royalsocietypublishing.org/doi/abs/10.1098/rspa.1964.0190>, doi:10.1098/rspa.1964.0190.
- [3] Junjiro Kanamori. Electron Correlation and Ferromagnetism of Transition Metals. *Prog. Theor. Phys.*, 30(3):275–289, 09 1963. doi:10.1143/PTP.30.275.
- [4] Martin C. Gutzwiller. Effect of Correlation on the Ferromagnetism of Transition Metals. *Phys. Rev. Lett.*, 10:159–162, Mar 1963. URL: <http://link.aps.org/doi/10.1103/PhysRevLett.10.159>, doi:10.1103/PhysRevLett.10.159.
- [5] Daniel P. Arovas, Erez Berg, Steven A. Kivelson, and Srinivas Raghu. The Hubbard Model. *Annual Review of Condensed Matter Physics*, 13(1):239–274, 2022. arXiv:<https://doi.org/10.1146/annurev-conmatphys-031620-102024>, doi:10.1146/annurev-conmatphys-031620-102024.
- [6] Mingpu Qin, Thomas Schäfer, Sabine Andergassen, Philippe Corboz, and Emanuel Gull. The Hubbard Model: A Computational Perspective. *Annual Review of Condensed Matter Physics*, 13(1):275–302, 2022. arXiv:<https://doi.org/10.1146/annurev-conmatphys-090921-033948>, doi:10.1146/annurev-conmatphys-090921-033948.
- [7] E. Kozik, E. Burovski, V. W. Scarola, and M. Troyer. Néel temperature and thermodynamics of the half-filled three-dimensional Hubbard model by diagrammatic determinant Monte Carlo. *Phys. Rev. B*, 87:205102, May 2013. URL: <https://link.aps.org/doi/10.1103/PhysRevB.87.205102>, doi:10.1103/PhysRevB.87.205102.
- [8] G. Rohringer, A. Toschi, A. Katanin, and K. Held. Critical Properties of the Half-Filled Hubbard Model in Three Dimensions. *Phys. Rev. Lett.*, 107:256402, Dec 2011. URL: <https://link.aps.org/doi/10.1103/PhysRevLett.107.256402>, doi:10.1103/PhysRevLett.107.256402.

- [9] P. R. C. Kent, M. Jarrell, T. A. Maier, and Th. Pruschke. Efficient calculation of the antiferromagnetic phase diagram of the three-dimensional Hubbard model. *Phys. Rev. B*, 72:060411, Aug 2005. URL: <https://link.aps.org/doi/10.1103/PhysRevB.72.060411>, doi: 10.1103/PhysRevB.72.060411.
- [10] J. Ehrlich and C. Honerkamp. Functional renormalization group for fermion lattice models in three dimensions: Application to the Hubbard model on the cubic lattice. *Phys. Rev. B*, 102:195108, Nov 2020. URL: <https://link.aps.org/doi/10.1103/PhysRevB.102.195108>, doi:10.1103/PhysRevB.102.195108.
- [11] Daniel Hirschmeier, Hartmut Hafermann, Emanuel Gull, Alexander I. Lichtenstein, and Andrey E. Antipov. Mechanisms of finite-temperature magnetism in the three-dimensional Hubbard model. *Phys. Rev. B*, 92:144409, Oct 2015. URL: <https://link.aps.org/doi/10.1103/PhysRevB.92.144409>, doi:10.1103/PhysRevB.92.144409.
- [12] R. Staudt, M. Dzierzawa, and A. Muramatsu. Phase diagram of the three-dimensional hubbard model at half filling. *The European Physical Journal B - Condensed Matter and Complex Systems*, 2000. doi:10.1007/s100510070120.
- [13] A. N. Tahvildar-Zadeh, J. K. Freericks, and M. Jarrell. Magnetic phase diagram of the Hubbard model in three dimensions: The second-order local approximation. *Phys. Rev. B*, 55:942–946, Jan 1997. URL: <https://link.aps.org/doi/10.1103/PhysRevB.55.942>, doi:10.1103/PhysRevB.55.942.
- [14] G. Rohringer and A. Toschi. Impact of nonlocal correlations over different energy scales: A dynamical vertex approximation study. *Phys. Rev. B*, 94:125144, Sep 2016. URL: <https://link.aps.org/doi/10.1103/PhysRevB.94.125144>, doi:10.1103/PhysRevB.94.125144.
- [15] Sergei Isakov and Emanuel Gull. Phase transitions in partial summation methods: Results from the three-dimensional Hubbard model. *Phys. Rev. B*, 105(4):045109, January 2022. arXiv:2110.06857, doi: 10.1103/PhysRevB.105.045109.
- [16] G. Rohringer, H. Hafermann, A. Toschi, A. A. Katanin, A. E. Antipov, M. I. Katsnelson, A. I. Lichtenstein, A. N. Rubtsov, and K. Held. Diagrammatic routes to nonlocal correlations beyond dynamical mean field theory. *Rev. Mod. Phys.*, 90:025003, May 2018. URL: <https://link.aps.org/doi/10.1103/RevModPhys.90.025003>, doi:10.1103/RevModPhys.90.025003.
- [17] Lorenzo Del Re and Alessandro Toschi. Dynamical vertex approximation for many-electron systems with spontaneously broken su(2) symmetry. *Phys. Rev. B*, 104:085120, Aug 2021. URL: <https://link.aps.org/doi/10.1103/PhysRevB.104.085120>, doi:10.1103/PhysRevB.104.085120.
- [18] Leticia Tarruell and Laurent Sanchez-Palencia. Quantum simulation of the Hubbard model with ultracold fermions in optical lattices. *Comptes Rendus Physique*, 19(6):365–393, 2018. Quantum simulation / Simulation quantique. URL: <https://www.sciencedirect.com/science/article/pii/S1631070518300926>, doi:https://doi.org/10.1016/j.crhy.2018.10.013.
- [19] Russell A. Hart, Pedro M. Duarte, Tsung-Lin Yang, Xinxing Liu, Thereza Paiva, Ehsan Khatami, Richard T. Scalettar, Nandini Trivedi, David A. Huse, and Randall G. Hulet. Observation of antiferromagnetic correlations in the Hubbard model with ultracold atoms. *Nature*, 519(7542):211–214, Mar 2015. doi:10.1038/nature14223.
- [20] Anton Mazurenko, Christie S. Chiu, Geoffrey Ji, Maxwell F. Parsons, Márton Kanász-Nagy, Richard Schmidt, Fabian Grusdt, Eugene Demler, Daniel Greif, and Markus Greiner. A cold-atom Fermi–Hubbard antiferromagnet. *Nature*, 545(7655):462–466, May 2017. doi:10.1038/nature22362.
- [21] Daniel Greif, Gregor Jotzu, Michael Messer, Rémi Desbuquois, and Tilman Esslinger. Formation and Dynamics of Antiferromagnetic Correlations in Tunable Optical Lattices. *Phys. Rev. Lett.*, 115:260401, Dec 2015. URL: <https://link.aps.org/doi/10.1103/PhysRevLett.115.260401>, doi:10.1103/PhysRevLett.115.260401.
- [22] Lawrence W Cheuk, Matthew A Nichols, Katherine R Lawrence, Melih Okan, Hao Zhang, Ehsan Khatami, Nandini Trivedi, Thereza Paiva, Marcos Rigol, and Martin W Zwierlein. Observation of spatial charge and spin correlations in the 2d fermi-hubbard model. *Science*, 353(6305):1260–1264, 2016.
- [23] Peter T Brown, Debayan Mitra, Elmer Guardado-Sanchez, Peter Schauß, Stanimir S Kondov, Ehsan Khatami, Thereza Paiva, Nandini Trivedi, David A Huse, and Waseem S Bakr. Spin-imbalance in a 2d fermi-hubbard system. *Science*, 357(6358):1385–1388, 2017.
- [24] Joannis Koepsell, Jayadev Vijayan, Pimonpan Sompert, Fabian Grusdt, Timon A Hilker, Eugene Demler, Guillaume Salomon, Immanuel Bloch, and Christian Gross. Imaging magnetic polarons in the doped fermi–hubbard model. *Nature*, 572(7769):358–362, 2019.
- [25] Marcell Gall, Nicola Wurz, Jens Samland, Chun Fai Chan, and Michael Köhl. Competing magnetic orders in a bilayer hubbard model with ultracold atoms. *Nature*, 589(7840):40–43, 2021.
- [26] Pimonpan Sompert, Sarah Hirthe, Dominik Bourgund, Thomas Chalopin, Julian Bibo, Joannis Koepsell, Petar Bojović, Ruben Verresen, Frank Pollmann, Guillaume Salomon, et al. Realizing the symmetry-protected haldane phase in fermi–hubbard ladders. *Nature*, pages 1–5, 2022.
- [27] Nikolai V. Prokof’ev and Boris V. Svistunov. Polaron Problem by Diagrammatic Quantum Monte Carlo. *Phys. Rev. Lett.*, 81:2514–2517, Sep 1998. URL: <https://link.aps.org/doi/10.1103/PhysRevLett.81.2514>, doi:10.1103/PhysRevLett.81.2514.
- [28] Kris Van Houcke, Evgeny Kozik, Nikolay Prokof’ev, and Boris Svistunov. *Phys. Procedia*, 6:95, 2010. doi:10.1016/j.phpro.2010.09.034.
- [29] E. Kozik, K. Van Houcke, E. Gull, L. Pollet, N. Prokof’ev, B. Svistunov, and M. Troyer. Diagrammatic monte carlo for correlated fermions. *Europhys. Lett.*, 90:10004, 2010. doi:10.1209/0295-5075/90/10004.
- [30] Riccardo Rossi. Determinant Diagrammatic Monte Carlo Algorithm in the Thermodynamic Limit. *Phys. Rev. Lett.*, 119:045701, Jul 2017. URL: <https://link.aps.org/doi/10.1103/PhysRevLett.119.045701>, doi:10.1103/PhysRevLett.119.045701.
- [31] R. Rossi, N. Prokof’ev, B. Svistunov, K. Van Houcke, and F. Werner. Polynomial complexity despite the fermionic sign. *EPL (Europhysics Letters)*, 118(1):10004, apr 2017. doi:10.1209/0295-5075/118/10004.

- [32] Fedor Šimkovic, J. P. F. LeBlanc, Aaram J. Kim, Youjin Deng, N. V. Prokof'ev, B. V. Svistunov, and Evgeny Kozik. Extended Crossover from a Fermi Liquid to a Quasiantiferromagnet in the Half-Filled 2D Hubbard Model. *Phys. Rev. Lett.*, 124:017003, Jan 2020. URL: <https://link.aps.org/doi/10.1103/PhysRevLett.124.017003>, doi:10.1103/PhysRevLett.124.017003.
- [33] Thomas Schäfer, Nils Wentzell, Fedor Šimkovic, Yuan-Yao He, Cornelia Hille, Marcel Klett, Christian J. Eckhardt, Behnam Arzhang, Viktor Harkov, François-Marie Le Régent, Alfred Kirsch, Yan Wang, Aaram J. Kim, Evgeny Kozik, Evgeny A. Stepanov, Anna Kauch, Sabine Andergassen, Philipp Hansmann, Daniel Rohe, Yuri M. Vilks, James P. F. LeBlanc, Shiwei Zhang, A.-M. S. Tremblay, Michel Ferrero, Olivier Parcollet, and Antoine Georges. Tracking the Footprints of Spin Fluctuations: A MultiMethod, MultiMessenger Study of the Two-Dimensional Hubbard Model. *Phys. Rev. X*, 11:011058, Mar 2021. URL: <https://link.aps.org/doi/10.1103/PhysRevX.11.011058>, doi:10.1103/PhysRevX.11.011058.
- [34] Aaram J. Kim, Fedor Simkovic, and Evgeny Kozik. Spin and Charge Correlations across the Metal-to-Insulator Crossover in the Half-Filled 2D Hubbard Model. *Phys. Rev. Lett.*, 124:117602, Mar 2020. URL: <https://link.aps.org/doi/10.1103/PhysRevLett.124.117602>, doi:10.1103/PhysRevLett.124.117602.
- [35] Connor Lenihan, Aaram J. Kim, Fedor Šimkovic IV., and Evgeny Kozik. Entropy in the Non-Fermi-Liquid Regime of the Doped 2D Hubbard Model. *Phys. Rev. Lett.*, 126:105701, Mar 2021. URL: <https://link.aps.org/doi/10.1103/PhysRevLett.126.105701>, doi:10.1103/PhysRevLett.126.105701.
- [36] J. P. F. LeBlanc, Andrey E. Antipov, Federico Becca, Ireneusz W. Bulik, Garnet Kin-Lic Chan, Chia-Min Chung, Youjin Deng, Michel Ferrero, Thomas M. Henderson, Carlos A. Jiménez-Hoyos, E. Kozik, Xuan-Wen Liu, Andrew J. Millis, N. V. Prokof'ev, Mingpu Qin, Gustavo E. Scuseria, Hao Shi, B. V. Svistunov, Luca F. Tocchio, I. S. Tupitsyn, Steven R. White, Shiwei Zhang, Bo-Xiao Zheng, Zhenyue Zhu, and Emanuel Gull. Solutions of the Two-Dimensional Hubbard Model: Benchmarks and Results from a Wide Range of Numerical Algorithms. *Phys. Rev. X*, 5:041041, Dec 2015. URL: <https://link.aps.org/doi/10.1103/PhysRevX.5.041041>, doi:10.1103/PhysRevX.5.041041.
- [37] Wei Wu, Michel Ferrero, Antoine Georges, and Evgeny Kozik. Controlling Feynman diagrammatic expansions: Physical nature of the pseudogap in the two-dimensional Hubbard model. *Phys. Rev. B*, 96:041105, Jul 2017. URL: <https://link.aps.org/doi/10.1103/PhysRevB.96.041105>, doi:10.1103/PhysRevB.96.041105.
- [38] Riccardo Rossi, Fedor Šimkovic, and Michel Ferrero. Renormalized perturbation theory at large expansion orders. *EPL (Europhysics Letters)*, 132(1):11001, 2020.
- [39] Fedor Šimkovic, Riccardo Rossi, and Michel Ferrero. The Weak, the Strong and the Long Correlation Regimes of the Two-Dimensional Hubbard Model at Finite Temperature. *arXiv e-prints*, page arXiv:2110.05863, October 2021. arXiv:2110.05863.
- [40] Connor Lenihan, Aaram J. Kim, IV. Šimkovic, Fedor, and Evgeny Kozik. Evaluating second-order phase transitions with Diagrammatic Monte Carlo: Néel Transition in the doped three-dimensional Hubbard model. *arXiv e-prints*, page arXiv:2112.15209, December 2021. arXiv:2112.15209.
- [41] Fedor Simkovic, Riccardo Rossi, Antoine Georges, and Michel Ferrero. URL: <https://arxiv.org/abs/2209.09237>, arXiv:arXiv:2209.09237, doi:10.48550/ARXIV.2209.09237.
- [42] Rosario E. V. Profumo, Christoph Groth, Laura Messio, Olivier Parcollet, and Xavier Waintal. Quantum Monte Carlo for correlated out-of-equilibrium nanoelectronic devices. *Phys. Rev. B*, 91:245154, Jun 2015. URL: <https://link.aps.org/doi/10.1103/PhysRevB.91.245154>, doi:10.1103/PhysRevB.91.245154.
- [43] Fedor Šimkovic, Riccardo Rossi, and Michel Ferrero. Efficient one-loop-renormalized vertex expansions with connected determinant diagrammatic Monte Carlo. *Phys. Rev. B*, 102:195122, Nov 2020. URL: <https://link.aps.org/doi/10.1103/PhysRevB.102.195122>, doi:10.1103/PhysRevB.102.195122.
- [44] Aaram J. Kim, Nikolay V. Prokof'ev, Boris V. Svistunov, and Evgeny Kozik. Homotopic Action: A Pathway to Convergent Diagrammatic Theories. *Phys. Rev. Lett.*, 126:257001, Jun 2021. URL: <https://link.aps.org/doi/10.1103/PhysRevLett.126.257001>, doi:10.1103/PhysRevLett.126.257001.
- [45] James P. F. LeBlanc, Kun Chen, Kristjan Haule, Nikolay V. Prokof'ev, and Igor S. Tupitsyn. Dynamic response of the electron gas: Towards the exact exchange-correlation kernel. URL: <https://arxiv.org/abs/2205.13595>, arXiv:arXiv:2205.13595, doi:10.48550/ARXIV.2205.13595.
- [46] R. Rossi, T. Ohgoe, K. Van Houcke, and F. Werner. Resummation of diagrammatic series with zero convergence radius for strongly correlated fermions. *Phys. Rev. Lett*, 121:130405, 2018. URL: <https://link.aps.org/doi/10.1103/PhysRevLett.121.130405>, doi:10.1103/PhysRevLett.121.130405.
- [47] K. Chen and K. Haule. A combined variational and diagrammatic quantum monte carlo approach to the many-electron problem. *Nature Comm.*, 10:3725, 2019. doi:10.1038/s41467-019-11708-6.
- [48] R. Rossi, F. Werner, N. Prokof'ev, and B. Svistunov. Shifted-action expansion and applicability of dressed diagrammatic schemes. *Phys. Rev. B*, 93:161102(R), 2016. doi:10.1103/PhysRevB.93.161102.
- [49] Igor S. Tupitsyn and Nikolay V. Prokof'ev. Phase diagram topology of the haldane-hubbard-coulomb model. *Phys. Rev. B*, 99:121113(R), 2019. URL: <https://link.aps.org/doi/10.1103/PhysRevB.99.121113>, doi:10.1103/PhysRevB.99.121113.
- [50] Yuan Huang, Kun Chen, Youjin Deng, Nikolay Prokof'ev, and Boris Svistunov. Spin-Ice State of the Quantum Heisenberg Antiferromagnet on the Pyrochlore Lattice. *Phys. Rev. Lett.*, 116:177203, 2016. doi:10.1103/PhysRevLett.116.177203.
- [51] G. Spada, R. Rossi, F. Simkovic, R. Garioud, M. Ferrero, K. Van Houcke, and F. Werner. High-order expansion around BCS theory. *arXiv e-prints*, page arXiv:2103.12038, March 2021. arXiv:2103.12038.
- [52] Fedor Šimkovic and Riccardo Rossi. Many-Configuration Markov-Chain Monte Carlo. *arXiv e-prints*, page arXiv:2102.05613, February 2021. arXiv:2102.05613.
- [53] Kent Griffin and Michael J. Tsatsomeris. Principal minors, Part I: A method for comput-

- ing all the principal minors of a matrix. *Linear Algebra and its Applications*, 419(1):107–124, 2006. URL: <https://www.sciencedirect.com/science/article/pii/S0024379506002126>, doi:<https://doi.org/10.1016/j.laa.2006.04.008>.
- [54] Fedor Šimkovic and Michel Ferrero. Fast principal minor algorithms for diagrammatic Monte Carlo. *Phys. Rev. B*, 105:125104, Mar 2022. URL: <https://link.aps.org/doi/10.1103/PhysRevB.105.125104>, doi:10.1103/PhysRevB.105.125104.
- [55] George A. Baker. Application of the Padé Approximant Method to the Investigation of Some Magnetic Properties of the Ising Model. *Phys. Rev.*, 124:768–774, Nov 1961. URL: <https://link.aps.org/doi/10.1103/PhysRev.124.768>, doi:10.1103/PhysRev.124.768.
- [56] Fedor Šimkovic and Evgeny Kozik. Determinant Monte Carlo for irreducible Feynman diagrams in the strongly correlated regime. *Phys. Rev. B*, 100:121102, Sep 2019. URL: <https://link.aps.org/doi/10.1103/PhysRevB.100.121102>, doi:10.1103/PhysRevB.100.121102.
- [57] See supplemental material at.
- [58] Julian Stobbe and Georg Rohringer. Consistency of potential energy in the dynamical vertex approximation. *Phys. Rev. B*, 106:205101, Nov 2022. URL: <https://link.aps.org/doi/10.1103/PhysRevB.106.205101>, doi:10.1103/PhysRevB.106.205101.
- [59] J. C. Slater. Magnetic Effects and the Hartree-Fock Equation. *Phys. Rev.*, 82:538–541, May 1951. URL: <https://link.aps.org/doi/10.1103/PhysRev.82.538>, doi:10.1103/PhysRev.82.538.
- [60] Anders W. Sandvik. Critical Temperature and the Transition from Quantum to Classical Order Parameter Fluctuations in the Three-Dimensional Heisenberg Antiferromagnet. *Phys. Rev. Lett.*, 80:5196–5199, Jun 1998. URL: <https://link.aps.org/doi/10.1103/PhysRevLett.80.5196>, doi:10.1103/PhysRevLett.80.5196.
- [61] Massimo Campostrini, Martin Hasenbusch, Andrea Pelissetto, Paolo Rossi, and Ettore Vicari. Critical exponents and equation of state of the three-dimensional Heisenberg universality class. *Phys. Rev. B*, 65:144520, Apr 2002. URL: <https://link.aps.org/doi/10.1103/PhysRevB.65.144520>, doi:10.1103/PhysRevB.65.144520.
- [62] T. Schäfer, A. A. Katanin, K. Held, and A. Toschi. Interplay of Correlations and Kohn Anomalies in Three Dimensions: Quantum Criticality with a Twist. *Phys. Rev. Lett.*, 119:046402, Jul 2017. URL: <https://link.aps.org/doi/10.1103/PhysRevLett.119.046402>, doi:10.1103/PhysRevLett.119.046402.
- [63] Antoine Georges and Werner Krauth. Physical properties of the half-filled Hubbard model in infinite dimensions. *Phys. Rev. B*, 48:7167–7182, Sep 1993. URL: <https://link.aps.org/doi/10.1103/PhysRevB.48.7167>, doi:10.1103/PhysRevB.48.7167.
- [64] F. Werner, O. Parcollet, A. Georges, and S. R. Hassan. Interaction-Induced Adiabatic Cooling and Antiferromagnetism of Cold Fermions in Optical Lattices. *Phys. Rev. Lett.*, 95:056401, Jul 2005. URL: <https://link.aps.org/doi/10.1103/PhysRevLett.95.056401>, doi:10.1103/PhysRevLett.95.056401.
- [65] Lorenzo De Leo, Corinna Kollath, Antoine Georges, Michel Ferrero, and Olivier Parcollet. Trapping and Cooling Fermionic Atoms into Mott and Néel States. *Phys. Rev. Lett.*, 101:210403, Nov 2008. URL: <https://link.aps.org/doi/10.1103/PhysRevLett.101.210403>, doi:10.1103/PhysRevLett.101.210403.
- [66] E. V. Gorelik, I. Titvinidze, W. Hofstetter, M. Snoek, and N. Blümer. Néel Transition of Lattice Fermions in a Harmonic Trap: A Real-Space Dynamic Mean-Field Study. *Phys. Rev. Lett.*, 105:065301, Aug 2010. URL: <https://link.aps.org/doi/10.1103/PhysRevLett.105.065301>, doi:10.1103/PhysRevLett.105.065301.
- [67] Sebastian Fuchs, Emanuel Gull, Lode Pollet, Evgeni Burovski, Evgeny Kozik, Thomas Pruschke, and Matthias Troyer. Thermodynamics of the 3D Hubbard Model on Approaching the Néel Transition. *Phys. Rev. Lett.*, 106:030401, Jan 2011. URL: <https://link.aps.org/doi/10.1103/PhysRevLett.106.030401>, doi:10.1103/PhysRevLett.106.030401.
- [68] C. Taranto, G. Sangiovanni, K. Held, M. Capone, A. Georges, and A. Toschi. Signature of antiferromagnetic long-range order in the optical spectrum of strongly correlated electron systems. *Phys. Rev. B*, 85:085124, Feb 2012. URL: <https://link.aps.org/doi/10.1103/PhysRevB.85.085124>, doi:10.1103/PhysRevB.85.085124.
- [69] L. Fratino, P. Sémon, M. Charlebois, G. Sordi, and A.-M. S. Tremblay. Signatures of the Mott transition in the antiferromagnetic state of the two-dimensional Hubbard model. *Phys. Rev. B*, 95:235109, Jun 2017. URL: <https://link.aps.org/doi/10.1103/PhysRevB.95.235109>, doi:10.1103/PhysRevB.95.235109.
- [70] E. V. Gorelik, I. Titvinidze, W. Hofstetter, M. Snoek, and N. Blümer. Néel Transition of Lattice Fermions in a Harmonic Trap: A Real-Space Dynamic Mean-Field Study. *Phys. Rev. Lett.*, 105:065301, Aug 2010. URL: <https://link.aps.org/doi/10.1103/PhysRevLett.105.065301>, doi:10.1103/PhysRevLett.105.065301.
- [71] Anne-Marie Daré, Y. M. Vilks, and A. M. S. Tremblay. Crossover from two- to three-dimensional critical behavior for nearly antiferromagnetic itinerant electrons. *Phys. Rev. B*, 53:14236–14251, Jun 1996. URL: <https://link.aps.org/doi/10.1103/PhysRevB.53.14236>, doi:10.1103/PhysRevB.53.14236.

Supplemental material for “Symmetry-broken perturbation theory to large orders in antiferromagnetic phases”

TUNING THE SHIFT α

We detail in this section the effect of the choice of the shift parameter on the series behaviour and discuss our method for selecting the optimal value of the α parameter. The expression of the perturbation Hamiltonian \hat{H}_ξ is given in Eq. 1 with ξ the expansion parameter. We parameterize $h = \alpha h_{MF}$ with h_{MF} the effective field which corresponds to the mean-field solution at interaction U and temperature T . The free parameter α modifies the intensity of the staggered field in the non-perturbed system. There is no limitation prohibiting choices of $\alpha > 1$, however, it was not beneficial in our studies and we limit ourselves to values of the shift $\alpha \in [0, 1]$. The value $\alpha = 1$ leads to a non-perturbed Hamiltonian $\hat{H}_{\xi=0}$ corresponding to the antiferromagnetic mean-field Hamiltonian for which the Hartree insertions are canceled in the diagrammatic expansion of an observable \mathcal{A} .

The choice of the value of the α parameter changes the non-interacting Hamiltonian \hat{H}_0 and therefore modifies the series behavior and its convergence properties. We illustrate in Fig. S1 the effect of the value of the shift parameter on the shape of the partial sums for different observables. The value of the α parameter leading to the best convergence of the partial sum depends on the parameters T and U of the computation and on the computed observable. If the best convergence is usually given by shifts in the range $\alpha \in [0.7-1]$, it is helpful (especially for the magnetization close to the Néel temperature) to calibrate its value in order to obtain a quickly converging partial sum. At $U = 4$, $T = 0.15$ we find a ‘magical shift’ $\alpha = 0.162$ for which the convergence of the series is optimal, leading to an accurate result. The maximum expansion order we are able to reach with good accuracy depends strongly on the value of the shift and is higher for α close to 1, which can be explained by the cancellation of Hartree insertion which reduces the MC variance.

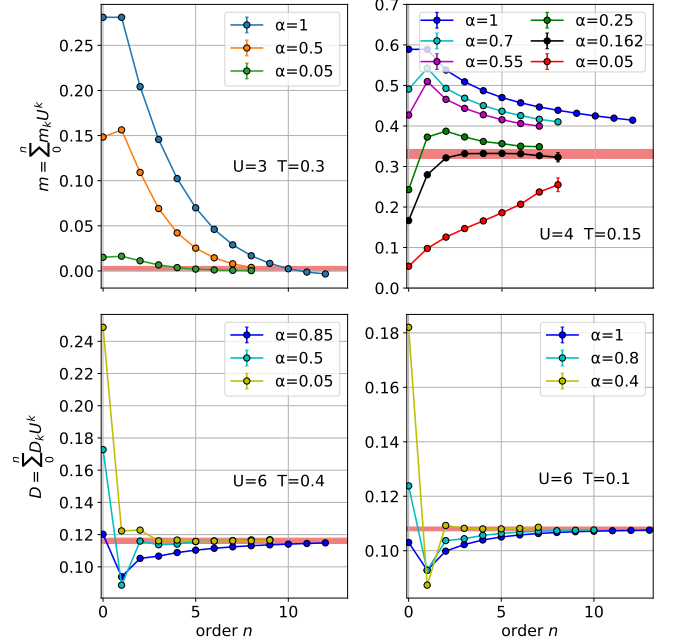


FIG. S1: Partial sums of magnetization m and double-occupancy D for different values of the interaction U and temperature T as a function of the maximum order n . The partial sums are highly dependent on the value of the shift α . The red colored band corresponds to the result with error after resummation.

We employ different resummation techniques in order to extrapolate the computed series to infinite orders. We use Padé and D-log Padé approximants [1, 2] cross checked with an exponential fitting of the expansion coefficient with respect to the order to establish a controlled result. In the end the error on an observable is determined through error propagation of the MC error on the expansion orders, after comparing the results from different resummations techniques, for at least two different values of the shift parameter α . We give in the Tables 1 2 3, the list of all the shifts α used for the purpose of this work in order to obtain controlled estimates of the double-occupancy, magnetization and grand potential density. For sets of parameters corresponding to the paramagnetic phase we also rely on non symmetry-broken expansions ($\alpha = 0$). For completeness we show in Fig. S2 a comparison of the resummation procedure which is used in this work (CDet(AF)) with the Fastest Apparent Convergence principle (FAC) resummation procedure used and described in details in [3]. The FAC procedure is based on optimizing the convergence of the expansion series with respect to the shift

parameter α according to the principle of minimal sensitivity [4–6]. Both resummation procedures give similar results with comparable errors.

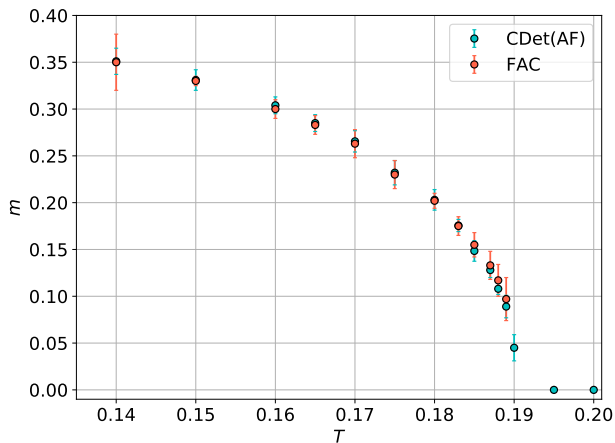


FIG. S2: Magnetization as a function of temperature at interaction $U = 4$ for different resummation procedures. The CDet(AF) data corresponds to the resummation procedure used in this work. See the main text for a description of the FAC resummation procedure.

SYSTEM-SIZE EFFECTS

The diagrammatic expansion is formulated directly in the thermodynamic limit. In practice we solve the unperturbed Hamiltonian and tabulate for finite L the non-interacting Green's functions to build the diagrammatic expansion of the problem. Considering an expansion series of the magnetization at $U = 4$, $T = 0.18$ close to the phase transition ($T_N \simeq 0.19$ at an interaction $U = 4$), we show in Fig. S3 that, up to relatively high order and negligible contribution to the resummed result, the contribution from each order is converged within statistical error for a linear system size $L \geq 20$. This shows that the final error on our results is dominated by statistical and resummation error. Finite size effects would only affect very high perturbation orders which can be neglected to determine the converging value of the series. This property remains valid when getting closer to the Néel temperature (see [7]). In our study, we fix the system-size to $L^3 = 20^3$ sites on a cubic lattice which proves to be large enough to avoid finite-size effects. To illustrate this we show the evolution of the value of different observables with linear system size in Fig. S4, with a convergence reached for $L \geq 20$.

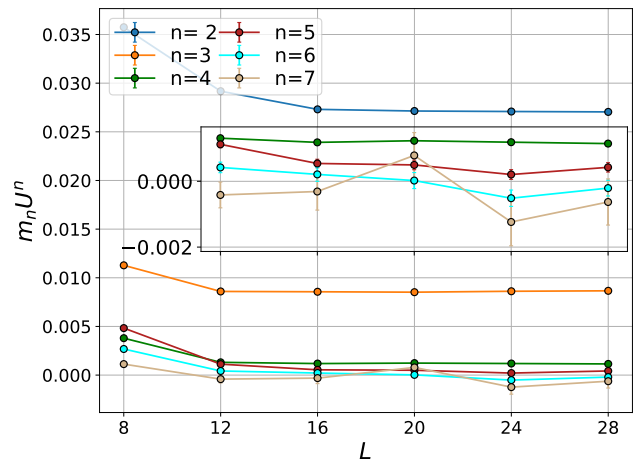


FIG. S3: System-size study : Contribution to the magnetization of its expansion coefficients m_n at different orders n , as a function of the linear system size L . The parameters of the perturbation expansion are $T = 0.18$, $U = 4$, $\alpha = 0.1$. The inset is the same plot for smaller contributions.

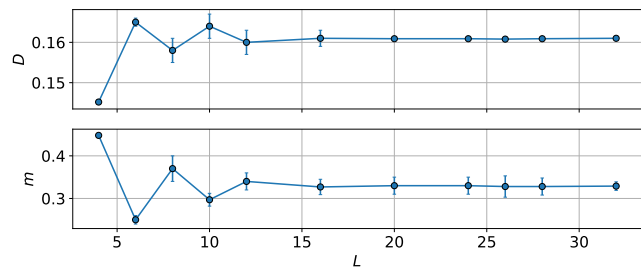


FIG. S4: System-size study : Double-occupancy and magnetization at $U = 4$, $T = 0.15$ as a function of the linear system size L for a cubic lattice of L^3 sites.

GRAND-POTENTIAL COMPUTATIONS

Grand potential computations are shown in Fig. S5. The corresponding magnetization is obtained with a first or second order polynomial fit of the grand potential data as a function of the external field H_{ext} . This method for estimating indirectly the magnetization as a derivative of the grand potential proves to be efficient deep inside the antiferromagnetic dome, in the regime where magnetization is saturated to its zero temperature value. In the vicinity of the phase transition we expect the grand potential curve as a function of the external field H_{ext} to

be flattening close to the origin $H_{\text{ext}} = 0$ as the temperature gets higher. These changes at very small fields are hard to resolve and we rely on direct computations of the magnetization in this regime.

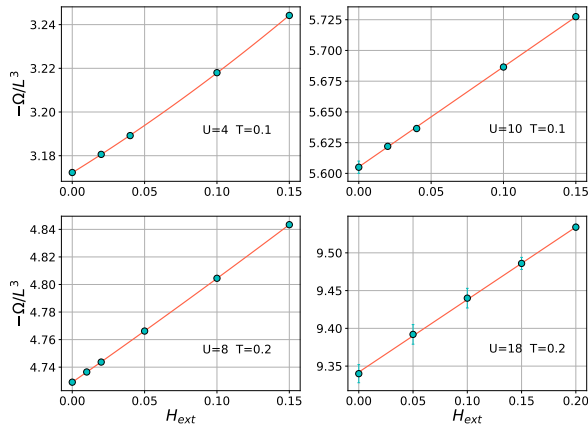


FIG. S5: Grand potential density $-\Omega/L^3$ as a function of the external staggered field H_{ext} for different values of the temperature and interaction parameters. The orange line corresponds to the best fit by a second (first) order polynomial on the top and bottom left (right) panels

T	U	α	T	U	α
0.1	3	(0.13,1)	0.2	7	(0.25,0.45,0.85)
0.2	3	(0.01,1)	0.3	7	(0.5,1)
0.3	3	(0.01,0.5)	0.1	8	(0.4,0.45,0.9)
0.05	4	(0.3,1)	0.15	8	(0.2,0.3,0.5)
0.075	4	(0.23)	0.2	8	(0.45,1)
0.1	4	(0.25,0.4,0.75)	0.25	8	(0.1,0.45,1)
0.125	4	(0.2,0.3,0.4,0.7)	0.3	8	(0.5,1)
0.15	4	(0.25,0.55,0.7)	0.325	8	(0.5,0.8)
0.16	4	(0.2,0.23,0.27)	0.35	8	(0.05,0.25,0.5)
0.17	4	(0.12,0.13,0.19)	0.375	8	(0.05,0.25,0.5)
0.18	4	(0.11,0.07)	0.4	8	(0.05,0.25,0.5)
0.19	4	(0.02)	0.1	9	(0.5,0.8)
0.195	4	(0,0.01)	0.2	9	(0.5,1)
0.2	4	(0.01,0.05)	0.3	9	(0.5,1)
0.21	4	(0.0001)	0.1	10	(0.4,0.5,1)
0.22	4	(0.0001)	0.2	10	(0.5,1)
0.225	4	(0.01,0.05)	0.3	10	(0.5,1)
0.23	4	(0.0001)	0.1	11	(0.5,1)
0.24	4	(0.0001)	0.2	11	(0.5,1)
0.25	4	(0.0001,0.05)	0.3	11	(0.5,1)
0.275	4	(0.01,0.05)	0.1	12	(0.5,1)
0.3	4	(0.0001,0.01,1)	0.2	12	(0.5,1)
0.325	4	(0.01)	0.3	12	(0.5,1)
0.35	4	(0.01,1)	0.1	13	(0.5,1)
0.4	4	(0.0001,1)	0.2	13	(0.5,1)
0.45	4	(0.0001,1)	0.3	13	(0.5,1)
0.5	4	(0.0001,1)	0.1	14	(0.5,1)
0.1	5	(0.2,0.4,0.8)	0.2	14	(0.5,1)
0.2	5	(0.2,0.4,0.5,0.8)	0.3	14	(0.5,1)
0.3	5	(0.1,0.5,1)	0.1	15	(0.5,1)
0.1	6	(0.4,0.8,1)	0.2	15	(0.5,1)
0.15	6	(0.75,1)	0.3	15	(0.5,1)
0.2	6	(0.45,0.83)	0.1	16	(0.5,1)
0.225	6	(0.65,1)	0.2	16	(0.5,1)
0.25	6	(0.6,1)	0.3	16	(0.5,1)
0.3	6	(0.5,1)	0.1	17	(0.5,1)
0.325	6	(0.05,0.5,0.85)	0.2	17	(0.5,1)
0.35	6	(0.05,0.5,0.85)	0.3	17	(0.5,1)
0.375	6	(0.05,0.5,0.85)	0.1	18	(0.5,1)
0.4	6	(0.05,0.5,0.85)	0.2	18	(0.5,1)
0.1	7	(0.1,0.4,0.85)	0.3	18	(0.5,1)

TABLE 1: List of the shift parameters α used to obtain the double-occupancy for different parameters T and U .

T	U	α
0.0175	2	(0.25,0.3)
0.02	2	(0.25,0.3)
0.0225	2	(0.23,0.24,0.25)
0.025	2	(0.2,0.23)
0.0275	2	(0.23,0.24)
0.03	2	(0.22,0.225)
0.0325	2	(0.21,0.22,0.23)
0.035	2	(0.19,0.2)
0.0375	2	(0.15,0.16,0.17)
0.04	2	(0.1,0.11,0.12)
0.0425	2	(0.01,0.05)
0.1	3	(0.12,0.125,0.13)
0.1	3.5	(0.18,0.17)
0.075	4	(0.18,0.19)
0.1	4	(0.171,0.175,0.18)
0.125	4	(0.167,0.17,0.2)
0.14	4	(0.161)
0.15	4	(0.157,0.162,0.17,0.25)
0.16	4	(0.14,0.148,0.15,0.2)
0.165	4	(0.138,0.139)
0.17	4	(0.12,0.13,0.19)
0.175	4	(0.1,0.11,0.12,0.13)
0.18	4	(0.05,0.07,0.08,0.1)
0.183	4	(0.078,0.082,0.084)
0.185	4	(0.05,0.07)
0.187	4	(0.053,0.057,0.061)
0.188	4	(0.05,0.051,0.0513,0.052)
0.189	4	(0.033,0.042,0.045)
0.19	4	(0.02,0.025)
0.195	4	(0.001,0.01)
0.2	4	(0.01,0.05)
0.225	4	(0.01,0.05)
0.25	4	(0.0001,0.05)
0.1	5	(0.14,0.17,0.22)
0.2	5	(0.16,0.25)
0.1	6	(0.7,0.8,1)
0.15	6	(0.7,1)
0.2	6	(0.7,1)
0.22	6	(0.7,1)
0.24	6	(0.18,0.22)
0.25	6	(0.2,0.25)
0.26	6	(0.1,0.12)
0.27	6	(0.19,0.18)
0.28	6	(0.17,0.173,0.177,0.18)
0.29	6	(0.17,0.175)
0.295	6	(0.162,0.17)
0.3	6	(0.14,0.15)
0.305	6	(0.13,0.14)
0.31	6	(0.13,0.145)
0.315	6	(0.01,0.02)
0.32	6	(0.01)
0.1	7	(0.4,0.65,0.8)

TABLE 2: List of the shift parameters α used to obtain the magnetization for different parameters T and U .

T	U	H_{ext}	α	T	U	H_{ext}	α
0.1	4	0.	(0.7,1)	0.2	10	0.15	(0.7,1)
0.1	4	0.02	(0.7,1)	0.1	11	0	(0.7,1)
0.1	4	0.04	(0.7,1)	0.1	11	0.05	(0.7,1)
0.1	4	0.1	(0.7,1)	0.1	11	0.1	(0.7,1)
0.1	4	0.15	(0.7,1)	0.1	11	0.15	(0.7,1)
0.11	4	0.	(0.6,0.7,1)	0.1	11	0.2	(0.7,1)
0.12	4	0.	(0.6,0.7,1)	0.2	11	0	(0.7,1)
0.13	4	0.	(0.6,0.7,1)	0.2	11	0.05	(0.7,1)
0.14	4	0.	(0.6,0.7,1)	0.2	11	0.1	(0.7,1)
0.15	4	0.	(0.05,0.5,0.7,1)	0.2	11	0.15	(0.7,1)
0.15	4	0.01	(0.05,0.5,0.7,1)	0.2	11	0.2	(0.7,1)
0.15	4	0.02	(0.05,0.5,0.7,1)	0.1	12	0	(0.7,1)
0.16	4	0.	(0.05,0.5)	0.1	12	0.05	(0.7,1)
0.25	4	0.	(0.05,0.5,0.7)	0.1	12	0.1	(0.7,1)
0.3	4	0.	(0.05,0.5,0.7)	0.1	12	0.15	(0.7,1)
0.35	4	0.	(0.05,0.5,0.7)	0.1	12	0.2	(0.7,1)
0.4	4	0.	(0.05,0.5,1)	0.2	12	0	(0.7,1)
0.45	4	0.	(0.05,0.5,1)	0.2	12	0.05	(0.7,1)
0.5	4	0	(0.05,0.5,1)	0.2	12	0.1	(0.7,1)
0.75	4	0	(0.05,0.5,1)	0.2	12	0.15	(0.7,1)
0.1	5	0.	(0.7,1)	0.2	12	0.2	(0.7,1)
0.1	5	0.02	(0.7,1)	0.1	13	0	(0.7,1)
0.1	5	0.04	(0.7,1)	0.1	13	0.05	(0.7,1)
0.1	5	0.1	(0.7,1)	0.1	13	0.1	(0.7,1)
0.1	5	0.15	(0.7,1)	0.1	13	0.15	(0.7,1)
0.2	5	0	(0.7,1)	0.1	13	0.2	(0.7,1)
0.2	5	0.02	(0.7,1)	0.2	13	0	(0.7,1)
0.2	5	0.04	(0.7,1)	0.2	13	0.05	(0.7,1)
0.2	5	0.1	(0.7,1)	0.2	13	0.1	(0.7,1)
0.2	5	0.15	(0.7,1)	0.2	13	0.15	(0.7,1)
0.1	6	0.	(0.7,1)	0.2	13	0.2	(0.7,1)
0.1	6	0.02	(0.7,1)	0.1	14	0	(0.7,1)
0.1	6	0.05	(0.7,1)	0.1	14	0.05	(0.7,1)
0.1	6	0.1	(0.7,1)	0.1	14	0.1	(0.7,1)
0.1	6	0.15	(0.7,1)	0.1	14	0.15	(0.7,1)
0.2	6	0.	(0.7,1)	0.1	14	0.2	(0.7,1)
0.2	6	0.005	(0.7,1)	0.2	14	0	(0.7,1)
0.2	6	0.01	(0.7,1)	0.2	14	0.05	(0.7,1)
0.2	6	0.015	(0.7,1)	0.2	14	0.1	(0.7,1)
0.2	6	0.02	(0.7,1)	0.2	14	0.15	(0.7,1)
0.2	6	0.025	(0.7,1)	0.2	14	0.2	(0.7,1)
0.1	7	0	(0.7,1)	0.1	15	0	(0.7,1)
0.1	7	0.02	(0.7,1)	0.1	15	0.05	(0.7,1)
0.1	7	0.04	(0.7,1)	0.1	15	0.1	(0.7,1)
0.1	7	0.1	(0.7,1)	0.1	15	0.15	(0.7,1)
0.1	7	0.15	(0.7,1)	0.1	15	0.2	(0.7,1)
0.2	7	0	(0.7,1)	0.2	15	0	(0.7,1)
0.2	7	0.02	(0.7,1)	0.2	15	0.05	(0.7,1)
0.2	7	0.04	(0.7,1)	0.2	15	0.1	(0.7,1)
0.2	7	0.1	(0.7,1)	0.2	15	0.15	(0.7,1)
0.2	7	0.15	(0.7,1)	0.2	15	0.2	(0.7,1)
0.1	8	0	(0.7,1)	0.1	16	0	(0.7,1)
0.1	8	0.02	(0.7,1)	0.1	16	0.05	(0.7,1)
0.1	8	0.04	(0.7,1)	0.1	16	0.1	(0.7,1)
0.1	8	0.1	(0.7,1)	0.1	16	0.15	(0.7,1)
0.1	8	0.15	(0.7,1)	0.1	16	0.2	(0.7,1)
0.2	8	0.	(0.7,1)	0.2	16	0	(0.7,1)
0.2	8	0.01	(0.7,1)	0.2	16	0.05	(0.7,1)
0.2	8	0.02	(0.7,1)	0.2	16	0.1	(0.7,1)
0.2	8	0.05	(0.7,1)	0.2	16	0.15	(0.7,1)
0.2	8	0.1	(0.7,1)	0.2	16	0.2	(0.7,1)
0.2	8	0.15	(0.7,1)	0.1	17	0	(0.7,1)
0.1	9	0	(0.7,1)	0.1	17	0.05	(0.7,1)
0.1	9	0.02	(0.7,1)	0.1	17	0.1	(0.7,1)
0.1	9	0.04	(0.7,1)	0.1	17	0.15	(0.7,1)
0.1	9	0.1	(0.7,1)	0.1	17	0.2	(0.7,1)
0.1	9	0.15	(0.7,1)	0.2	17	0	(0.7,1)
0.2	9	0	(0.7,1)	0.2	17	0.05	(0.7,1)
0.2	9	0.02	(0.7,1)	0.2	17	0.1	(0.7,1)
0.2	9	0.04	(0.7,1)	0.2	17	0.15	(0.7,1)
0.2	9	0.1	(0.7,1)	0.2	17	0.2	(0.7,1)
0.2	9	0.15	(0.7,1)	0.1	18	0	(0.7,1)
0.1	10	0	(0.7,1)	0.1	18	0.05	(0.7,1)
0.1	10	0.02	(0.7,1)	0.1	18	0.1	(0.7,1)
0.1	10	0.04	(0.7,1)	0.1	18	0.15	(0.7,1)
0.1	10	0.1	(0.7,1)	0.1	18	0.2	(0.7,1)
0.1	10	0.15	(0.7,1)	0.2	18	0	(0.7,1)
0.2	10	0	(0.7,1)	0.2	18	0.05	(0.7,1)
0.2	10	0.02	(0.7,1)	0.2	18	0.1	(0.7,1)
0.2	10	0.04	(0.7,1)	0.2	18	0.15	(0.7,1)
0.2	10	0.1	(0.7,1)	0.2	18	0.2	(0.7,1)

TABLE 3: List of the shift parameters α used to obtain the grand potential density for different parameters T , U and H_{ext} .

-
- [1] F. Šimkovic and E. Kozik, “Determinant monte carlo for irreducible feynman diagrams in the strongly correlated regime,” *Phys. Rev. B*, vol. 100, p. 121102, Sep 2019.
- [2] G. A. Baker, “Application of the padé approximant method to the investigation of some magnetic properties of the ising model,” *Phys. Rev.*, vol. 124, pp. 768–774, Nov 1961.
- [3] G. Spada, R. Rossi, F. Simkovic, R. Garioud, M. Ferrero, K. Van Houcke, and F. Werner, “High-order expansion around BCS theory,” *arXiv e-prints*, p. arXiv:2103.12038, Mar. 2021.
- [4] J.-L. Kneur, M. B. Pinto, and R. O. Ramos, “Asymptotically improved convergence of optimized perturbation theory in the bose-einstein condensation problem,” *Phys. Rev. A*, vol. 68, p. 043615, Oct 2003.
- [5] P. M. Stevenson, “Optimized perturbation theory,” *Phys. Rev. D*, vol. 23, pp. 2916–2944, Jun 1981.
- [6] R. L. S. Farias, G. Krein, and R. O. Ramos, “Applicability of the linear δ expansion for the $\lambda\phi^4$ field theory at finite temperature in the symmetric and broken phases,” *Phys. Rev. D*, vol. 78, p. 065046, Sep 2008.
- [7] G. Spada, R. Rossi, F. Simkovic, R. Garioud, M. Ferrero, K. Van Houcke, and F. Werner, “High-order expansion around BCS theory,” *arXiv e-prints*, p. arXiv:2103.12038, Mar. 2021.